[1]K.A. Kuterbekov, [1]K.Zh. Bekmyrza, [1]A.M. Kabyshev,
[1]M.M. Kubenova, [1]N.K. Aidarbekov, [2]S.A. Nurkenov

[1]L.N. Gumilyov Eurasian National University, Astana, Kazakhstan;
[2]Astana International University, Astana, Kazakhstan
(E-mail: kbekmyrza@yandex.kz)

Investigation of the Characteristics of Materials with the Ruddlesden-Popper Structure for Solid Oxide Fuel Cells

This article presents the results of a study of the characteristics of materials based on lanthanum nickelate $La_2Ni_{1-x}Co_xO_{4+\delta}$ ($0 \leq x \leq 0.3$) and $Pr_2NiO_{4+\delta}$. Their crystal structure and interaction with YSZ and GDC electrolyte materials at 900 °C are analyzed. The thermal expansion coefficients are determined and the temperature dependences of the conductivities are studied. The polarization resistance of these materials in contact with the electrolyte material YSZ is also measured. As a result of the study, the following cathode materials were investigated: $La_2Ni_{1-x}Co_xO_4$ ($0 \leq x \leq 0.3$), Pr_2NiO_4. In this case, the influence of low concentrations of Co on the characteristics of lanthanum nickelate was studied for the first time. Materials based on lanthanum nickelate and praseodymium nickelate were characterized by a structure of the K_2NiF_4 type (Ruddlesden-Popper phases) with rhombic symmetry. A study of the thermal expansion of cathode materials showed that all the studied materials are characterized by higher CTEs than YSZ and GDC electrolytes. Based on the studies performed, cathode materials were chosen for the formation of composites with GDC electrolyte: La_2NiO_4, $La_2Ni_{0.8}Co_{0.2}O_4$, Pr_2NiO_4. A study of the sintering kinetics and CTE of composites showed that their thermal characteristics are much closer to those of electrolytes than those of pure cathode materials.

Key words: SOFC, cathode materials, conductivity, thermal expansion coefficient, nanopowders.

Introduction

Solid oxide fuel cells (SOFCs) are promising electrochemical devices that directly convert the chemical energy of a fuel into electrical and thermal energy. The main advantages of SOFC are the high theoretical efficiency of energy conversion (up to 60 % when using only electric power and up to 90 % when using combined electric and thermal energy) and environmental friendliness. In this regard, scientific and technological issues related to the creation of SOFC are widely studied. At the same time, an important task remains to increase the specific power of the cells, which directly depends on their internal resistance, which consists of the ohmic resistance of the electrolyte layers and electrodes, as well as polarization losses due to electrochemical processes on the electrodes. Thus, to reduce the internal resistance of SOFC, it is desirable to reduce both of these components.

One of the possible solutions to this problem is the creation of a non-porous cathode-electrolyte structure instead of the generally accepted one — porous cathode — dense electrolyte. In this case, the layer of cathode material, as well as the electrolyte, will prevent the mixing of fuel and oxidizing gases, which will reduce the thickness of the electrolyte layer and, consequently, its contribution to the internal resistance of SOFC.

Research methodology

Source materials

The initial nanosized powders of $Zr_{0.84}Y_{0.16}O_{2-\delta}$ (YSZ) and $Ce_{0.73}Gd_{0.27}O_{3-\delta}$ (GDC) electrolyte materials were obtained by laser evaporation [1].

Cathode materials, both with a perovskite structure based on praseodymium ferro-cobaltite, and with a Ruddlesden-Popper structure based on lanthanum nickelate and Pr_2NiO_4, were fabricated by the method of self-propagating high-temperature synthesis (SHS). The synthesis process was based on a variant of the Peccini method described in [2]. The reagents used were $Pr(NO_3)_3$ (analytical grade), $Fe(NO_3)_3$ (analytical grade), $Co(NO_3)_2$ (chemically pure), La_2O_3 (chemically pure), NiO (analytical grade), and $SrCO_3$ (analytical grade). Stoichiometric mixtures of reagents were dissolved in a 0.1 N HNO_3 solution until a homogeneous solution was obtained, which was evaporated to wet salts. As a combustible organic substance, a twofold volume of ethylene glycol $HOCH_2CH_2OH$ (chemically pure) was used, which was both a solvent and a rea-

gent. The reaction mixture was heated until the development of the SHS process. The reaction products were remixed and annealed step by step to remove residual organic phases at temperatures of 400, 700, and 900 °C with holding for 6 hours for each temperature. The final stage of processing was annealing at 1100 °C for 30 min.

Characteristics of source materials

The specific surface of the synthesized powders was determined by low-temperature nitrogen vapor sorption by the BET method on an automatic analyzer TriStar 3000. The measurement results are presented in Table 1.

The morphology of the obtained powders was studied by electron microscopy using a JEOL JEM 2100 transmission electron microscope and LEO 982 and JEOL JSM-6390LA scanning electron microscopes.

Figure 1 shows micrographs of the initial YSZ and GDC solid electrolyte powders. The particles of YSZ powder obtained by laser evaporation have a shape close to spherical. GDC powder particles are closer in shape to cubes rounded along the edges. At the same time, microscopy confirms the estimate of the average particle size of powders made on the basis of S_{BET}: about 15 nm for YSZ and 25 nm for GDC.

Micrographs of powders of cathode materials are shown in Figure 2. Powder particles obtained by SHS are irregularly shaped agglomerates. The average particle sizes determined by the BET method (Table 1) correlate with microscopy data.

Table 1

Nomenclature and characteristics of initial powders

Designation	Chemical composition	S_{BET}, m^2/g	d_{BET}, nm	Structure
Electrolyte materials				
YSZ	$Zr_{0,84}Y_{0,16}O_{2-\delta}$	48.1	21.0	Fluorite
GDC	$Ce_{0,73}Gd_{0,23}O_{2-\delta}$	34.2	24.3	Fluorite
Cathode materials				
LN	La_2NiO_4	2.71	320	Ruddlesden Popper
LNC-10	$La_2Ni_{0,9}Co_{0,1}O_4$	2.45	350	Ruddlesden Popper
LNC-20	$La_2Ni_{0,8}Co_{0,2}O_4$	3.05	270	Ruddlesden Popper
LNC-30	$La_2Ni_{0,7}Co_{0,3}O_4$	2.44	340	Ruddlesden Popper
PN	Pr_2NiO_4	1.71	490	Ruddlesden Popper

The phase composition of powders of electrolyte materials was determined by X-ray phase analysis performed on a D8 DISCOVER diffractometer using copper radiation (Cu K$_{\alpha1.2}$ λ = 1.542 Å) with a graphite monochromator using a diffracted beam. Processing was performed using the TOPAS 3 program with the Rietveld algorithm for refinement of structural parameters. When estimating the average crystallite size, we used the correction factor K (in the Scherer formula) = 0.89. The phase composition of the cathode materials during synthesis was monitored using a Shimadzu XRD-7000 S X-ray diffractometer. The X-ray patterns were processed using the FULLPROF program.

a)

b)
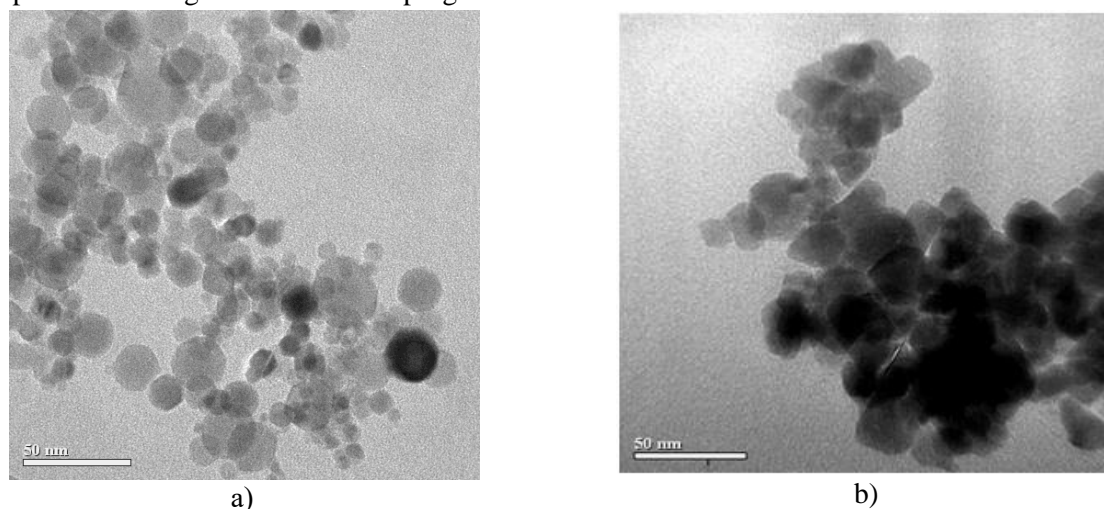
Figure 1. Micrographs of the initial powders of solid electrolytes (a) YSZ and b) GDC

Powders of electrolyte materials YSZ and GDC are single-phase and are solid solutions with space group Fm-3m. The cubic lattice parameters a were 5.143 and 5.424 Å for YSZ and GDC, respectively. X-ray phase analysis of powders of cathode materials showed that they are mostly single-phase, but there are traces (less than 2 %) of unidentified secondary phases. Perovskite cathode materials based on praseodymium ferrocobaltite had a rhombic structure after the synthesis procedure, while materials based on lanthanum nickelate and praseodymium nickelate were characterized by a structure of the K_2NiF_4 type.

Study of the structure and interaction with electrolytes.

Disk samples 15 mm in diameter were made from the initial powders to study the structure of dense ceramics. The powders were pressed on a uniaxial hydrostatic press PG30 UHL4. Sintered at 1400 °C for 10 hours.

Samples for studying the chemical interaction between cathode and electrolyte materials were prepared according to the following procedure. The required powders were mixed in a weight ratio of 1:1. They were filled with isopropyl alcohol and sonicated with a UZG8-0.4/22 disperser for 10 min. This procedure makes it possible to "break up" the agglomerates formed in nanosized powders and ensure a uniform distribution of the powders throughout the suspension. Further mixing was carried out using a gravity mixer for 2 days. YSZ balls were added to the slurry as interfering bodies. The resulting mixtures were dried with constant stirring using an RH B S000 (IKA) magnetic stirrer. The resulting mixtures were compacted using a uniaxial press into discs 10 mm in diameter and ~2 mm high. Then the disk samples were sintered at a certain temperature (Tables 3, 4) with an exposure of 5 hours.
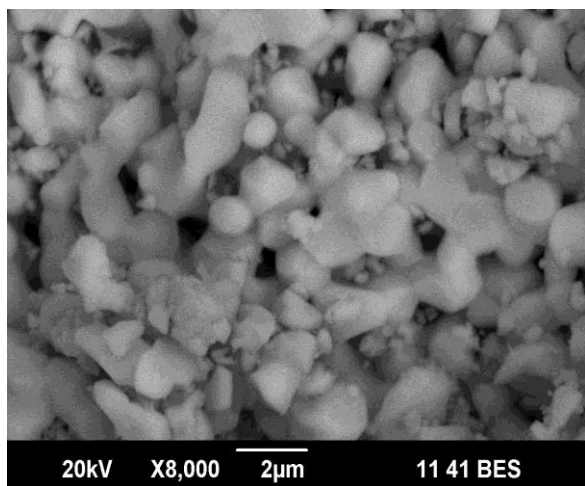
a)
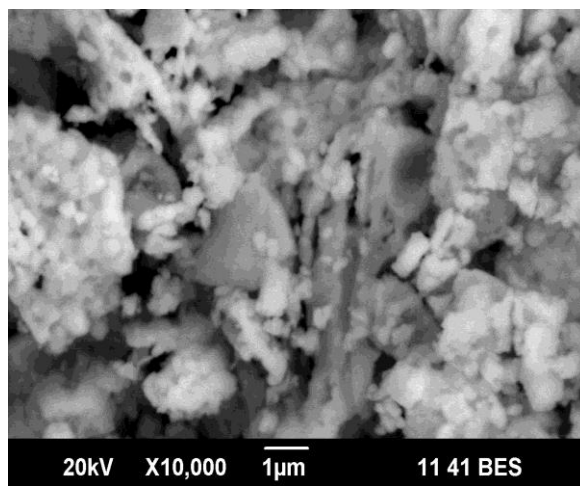
b)
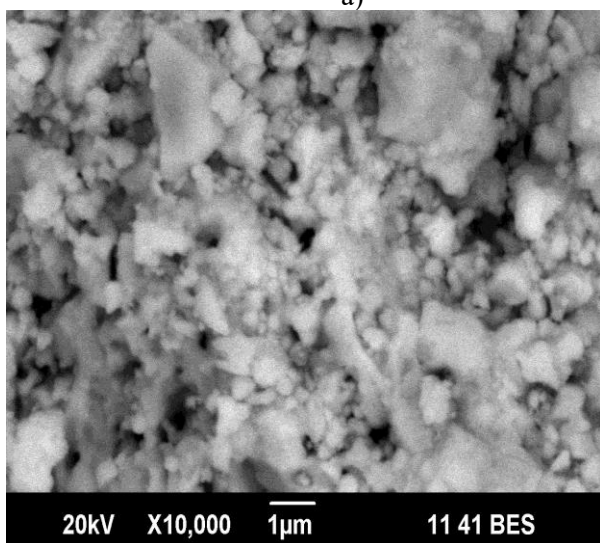
c)
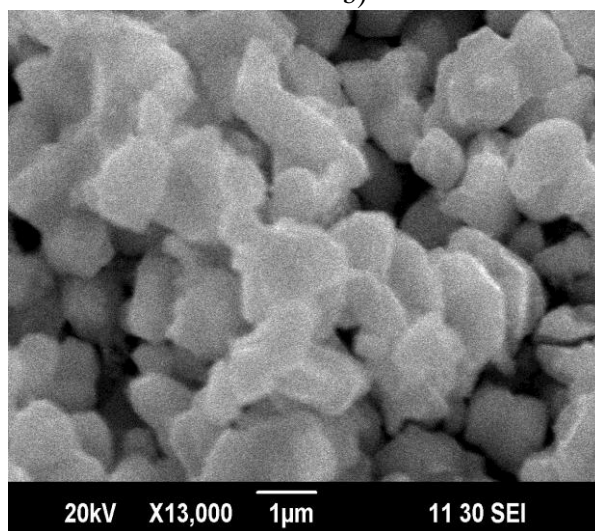
d)
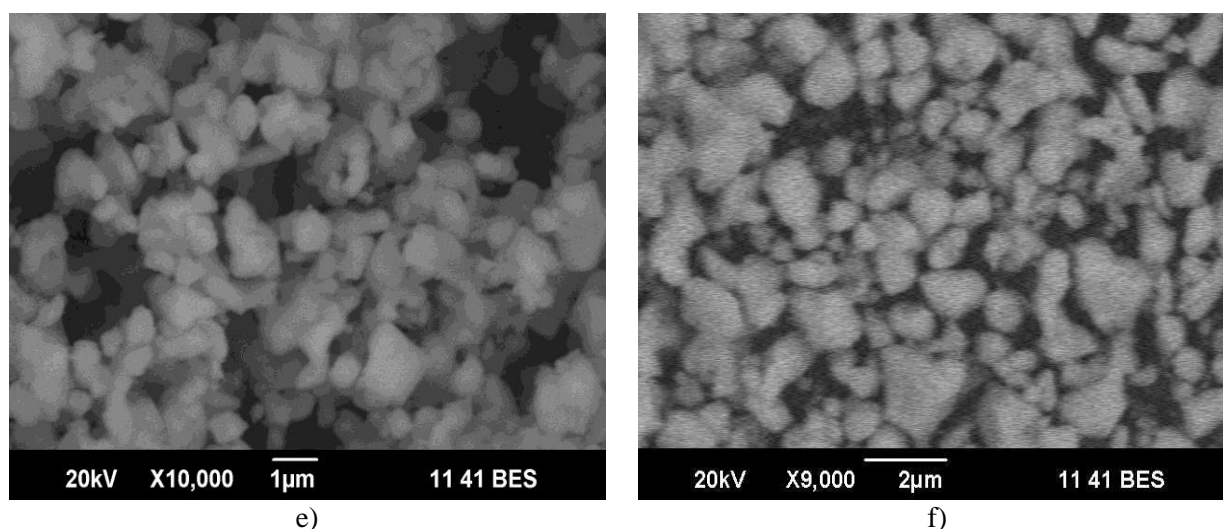
Figure 2. Micrographs of initial powders of cathode materials: a) $PrFe_{0.8}Co_{0.2}O_3$, b) $Pr_{0.7}Sr_{0.3}Fe_{0.8}Co_{0.2}O_3$, c) $Pr_{0.7}Sr_{0.3}Fe_{0.5}Co_{0.5}O_3$, d) La_2NiO_4, e) $La_2Ni_{0.8}Co_{0.2}O_4$, f) Pr_2NiO_4

The phase composition of samples of cathode materials and mixtures was determined by X-ray phase analysis performed on a diffractometer. Processing was performed using the TOPAS 3 program with the Rietveld algorithm for refinement of structural parameters.

Study of the coefficient of thermal expansion

The measurement of the linear expansion of cathode materials was carried out on samples in the form of bars with characteristic dimensions of $4 \times 4 \times 9.5$ mm, which were preliminarily sintered to densities close to theoretical (1400 °C, holding for 10 h).

Determination of the thermal expansion coefficient (TEC) of the samples was carried out in an air atmosphere in the temperature range of 20-1200 °C. The measurements were performed on a Dil 402C dilatometer. The heating rate was 5 °C per minute.

Conductivity study

To measure the conductivity, powders of cathode materials were pressed into rectangular bars with characteristic dimensions of $3\times2\times30$ mm. The samples were compacted using a PG30 UHL4 press. The resulting compacts were sintered in an air atmosphere. The sintering temperature of the samples is 1400 °C. The holding time was 10 h.

The density of sintered samples was determined by hydrostatic weighing.

Probes made of platinum wire with a diameter of 0.2 mm were deposited on the sintered samples. To ensure good electrical contact between the probes and the sample, the probes were smeared with platinum paste, which was baked at 1000 °C for 1 h.

Conductivity was measured in air by a 4-probe method at direct current in the temperature range of 20–950 °C using a Solartron Sl-1260/1287 impedance meter. The measurements were carried out in the potentiodynamic mode ($U_{max} = 0.1$ V).

Study of polarization resistance

The determination of the polarization resistance of cathode materials in contact with the YSZ electrolyte was performed on symmetrical samples.

Disk samples of YSZ carrier electrolyte were obtained by uniaxial pressing using a PG30 UHL4 press and subsequent sintering at a temperature of 1200 °C with a holding time of 6 hours. The characteristic dimensions of the resulting disk samples are: diameter, 12 mm; thickness, 1 mm. The density of the disk samples was at least 98 % of the theoretical density ($\gamma_{XRD\,YSZ}$=5.92 g/cm^3).

The electrodes under study were applied symmetrically on both sides of the YSZ disk samples by staining. The electrode diameter was 8 mm. To apply the electrodes, cathode pastes were prepared by mixing the initial cathode powders (90 wt.%) and rosin (10 wt.%) as a binder. The solvent was isopropyl alcohol. The

sintering temperatures of the electrodes varied from 900 to 1100 °C with an exposure of 1 hour. The thickness of the electrode layers was about 0.1 mm.

Symmetrical samples prepared as described above (Figure 3) for measuring the polarization resistance were placed in a measuring cell, in which they were clamped between platinum grids (Figure 4). Each grid has two probes (potential and current) made of platinum wire 0.5 mm in diameter. The measuring cell was placed in a tubular furnace, which allows you to set the temperature of the samples in the range of 20–900 °C.
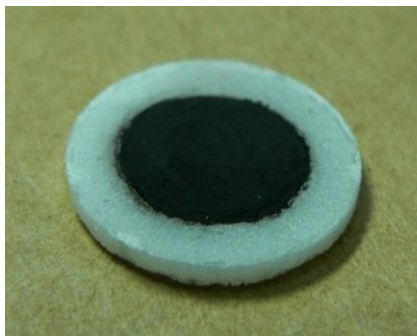
Figure 3. Appearance of the sample for research.
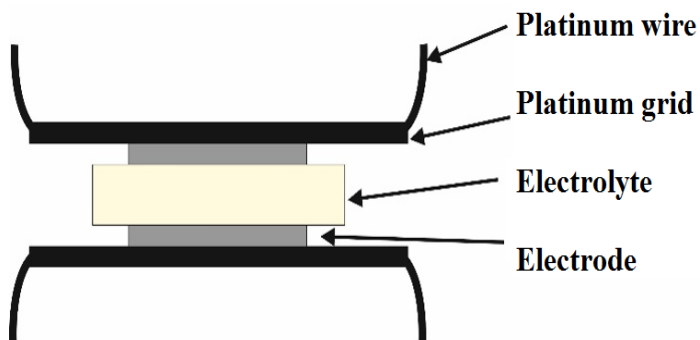
Figure 4. Diagram of a measuring cell for studying the polarization resistance of cathodes.

The impedance spectra were recorded at a voltage of 15 mV in the frequency range of 1 MHz–0.1 Hz using a Solartron Sl-1260/1287. The measurements were carried out in stagnant air in the temperature range of 850–650 °C.

The resulting impedance spectra were calculated using the equivalent circuit shown in Figure 5 using the ZView program. Where R_1 corresponds to the so-called series resistance, which includes the ohmic resistance of the electrolyte, probes. The resistance R_2 corresponds to the polarization resistance of the electrodes under study. Taking into account the fact that there are two identical electrodes in the measured system, the polarization resistance R_η was determined as half of R_2.
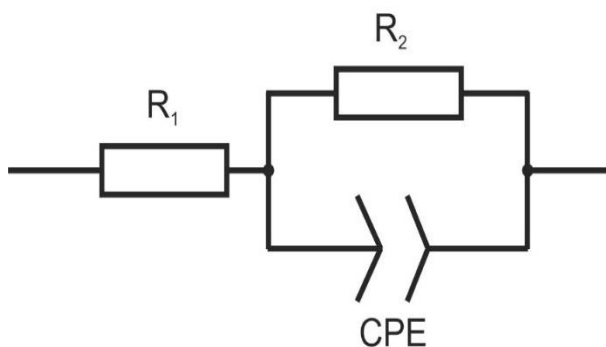
Figure 5. Equivalent circuit for calculating impedance spectra.

Experimental results

Crystal structure

On Figure 6 X-ray diffraction patterns of samples of cathode materials based on lanthanum nickelate and praseodymium nickelate sintered at 1400 °C are presented. Table 2 shows their crystallographic data.
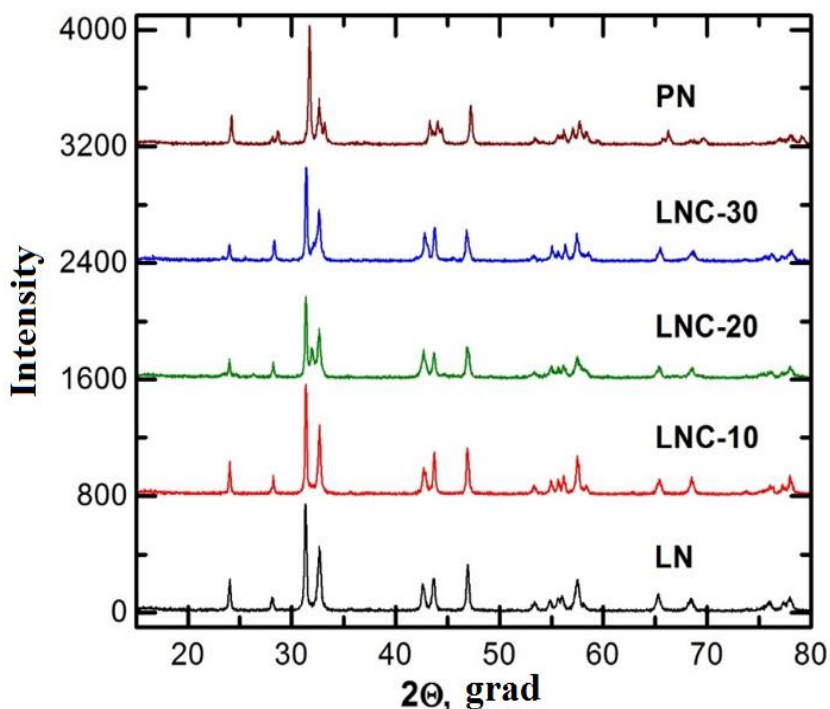
Figure 6. X-ray diffraction patterns of materials La$_2$Ni$_{1-x}$Co$_x$O$_4$, and Pr$_2$NiO$_4$.

All samples have a structure of the K$_2$NiF$_4$ type. In this case, the main type of symmetry of solid solutions is rhombic Fmmm. However, the LNC samples with 20 and 30 % Co also contain about 10 % of the tetragonal structure of the P4/m type, as well as trace structures symmetry of which can be identified as F4/mmm and R-3cH for LNC-20 and LNC-30, respectively. The PN material contains a sufficiently large amount of the structure with the P42/ncmZ symmetry corresponding to the formula Pr$_2$NiO$_{4.2}$, i.e. containing an excess amount of oxygen.

T a b l e 2

Crystallographic data of La$_2$Ni$_{1-x}$Co$_x$O$_4$ and Pr$_2$NiO$_{4+\delta}$ compositions.

Material	Space group	a, Å	b, Å	c, Å	Reference
		This work			
LN	100 % Fmmm	5.465(3)	5.489(3)	12.679(7)	
LNC-10	100 % Fmmm	5.469(3)	5.487(3)	12.639(5)	
LNC-20	88 % Fmmm 12 % P4/m	5.491(5) 11.149(9)	5.466(5)	12.637(9) 3.986(4)	
LNC-30	91 % Fmmm 9 % P4/m	5.492(3) 11.147(7)	5.473(3)	12.595(6) 3.883(4)	
PN	69 % Fmmm 31 % P42/ncmZ	5.482(3) 5.452(3)	5.391(3)	12.433(5) 12.438(8)	
		Literature data			
La$_2$NiO$_{4+\delta}$	Fmmm	5.4499	5.4574	12.6724	[3]
La$_2$CoO$_{4,1}$		5.543	5.493	12.684	[4]

The X-ray density determined for the LN composition is 6.995 g/cm^3.

- ○ A-site cation
- ● B-site cation
- ● Anion

$A_2BO_{4+\delta}$
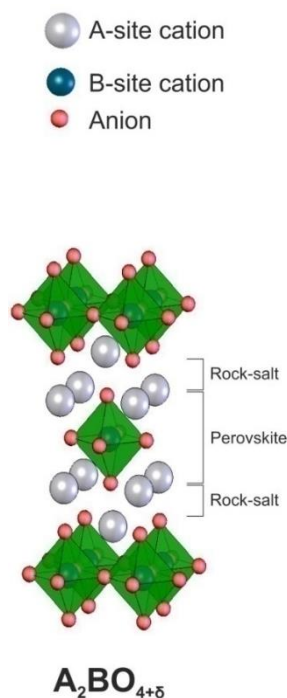
Figure 7. Ideal structure of Ruddlesden-Popper phases.

It is known from the literature [4-6] that in the high-temperature region $La_2MO_{4+\delta}$ materials are characterized by the tetragonal structure I4/mmm. In this state, the MO_6 octahedra are perfectly aligned along the c axis (Figure 7). As the temperature decreases, the structure is deformed, which is expressed in the cooperative deviation of the octahedra from the c axis, leading to the rhombic structure Fmmm. The transition temperature from Fmmm to I4/mmm for the $La_2NiO_{4+\delta}$ material is estimated at about 425 °C in [5] and about 200 °C in [6]. Whereas for the $La_2CoO_{4+\delta}$ material, the transition temperature to the I4/mmm structure is about 580 °C [4]. The literature data on the parameters of elementary cells given in Table 2 are close to the values obtained in our study.

As can be seen from Table 2 with an increase in the content of cobalt in the composition of lanthanum nickelate, there is a slight increase in the parameter a, and a decrease in the parameters b and c. These data correlate with the data of [7], where the compositions $La_2Ni_{1-x}Co_xO_{4+\delta}$ were also obtained by the Peccini method, but the symmetry of the solid solutions was determined as F4/mmm. Thus, the introduction of cobalt leads to structural distortions. Moreover, the data obtained, together with the dependence of δ on the cobalt content [8], allow us to state that the c-parameter is strongly related to the electronic state of cobalt ions. Thus, it was suggested in [9] that the decrease in c is due to the replacement of the high-spin Ni^{2+} ion (r_i=0.69 Å at CN=6) by a much smaller low-spin Co^{3+} ion (r_i=0.545 Å at CN=6).

In addition, a decrease in the c parameter with the introduction of Co can also be interpreted as an increase in the "thickness" of the rock salt layer along this direction [10]. Thus, this increase can be expected to lead to an improvement in the mobility of oxide ions in the ab plane.

Chemical interaction with electrolytes.

On Figure 8 shows X-ray diffraction patterns for mixtures of Ruddlesden-Popper electrolyte and cathode materials that were sintered at 900 °C for 5 hours. For comparison, in Figure 8 also shows separate X-ray diffraction patterns of electrolyte (YSZ and GDC) and cathode (LN, LNC-30 and PN) cathode materials. The results of the analysis of X-ray phase data are summarized in Table 3.

The data in Table 3 confirm the well-established opinion that the CeO_2-based electrolyte is more chemically Table to interaction with cathode materials than the ZrO_2-based electrolyte [11, 12]. Literature data also confirm rather high chemical activity of La_2NiO_4 towards YSZ, and Pr_2NiO_4 towards both YSZ and GDC [13-15]. For example, in [14], secondary phases $La_2Zr_2O_7$, $La_3Ni_2O_7$ were found in a mixture of lanthanum nickelate and YSZ after 2 h exposure at 900°C. Whereas no interaction was found with the GDC electrolyte under the same conditions [14]. Exposure for 24 hours at 900 °C of a mixture of Pr_2NiO_4 and

GDC led to the formation of $Pr_4Ni_3O_{10}$ and Pr_6O_{11}, while in a mixture with YSZ, $Pr_2Zr_2O_7$ was additionally formed at a similar exposure [15].

It is also believed that an increase in the content of cobalt in the composition of the cathode material increases its chemical activity with respect to the electrolyte material [12, 16]. Data on the interaction of LN and LNC-20 with GDC electrolyte confirm this pattern. However, it is unexpected that the introduction of Co into the composition of lanthanum nickelate seems to reduce the chemical activity with respect to the YSZ electrolyte (lower content of the secondary phase according to XRD data). The reasons for this behavior are currently unclear and require further research.

a)

b)

c)
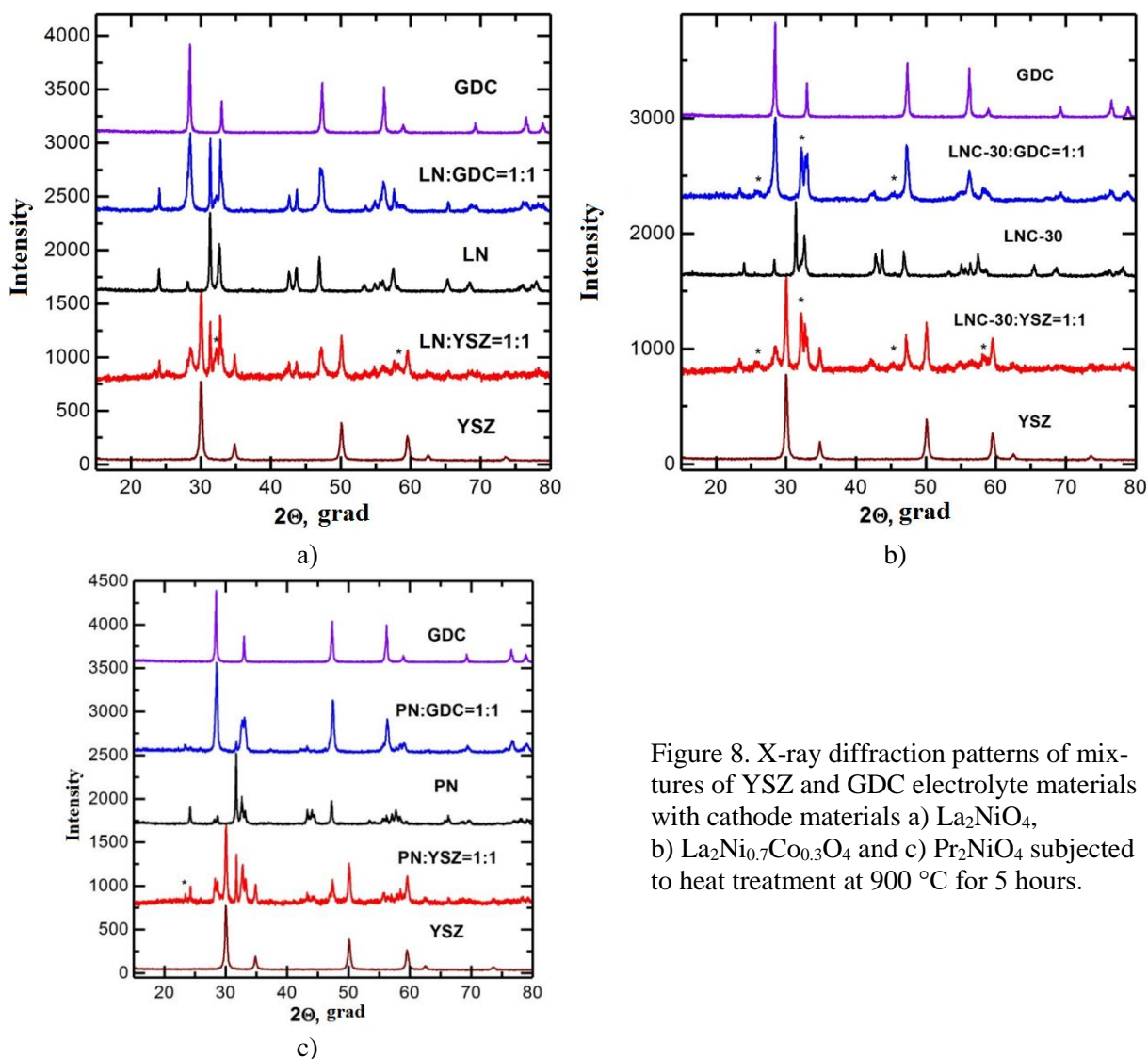
Figure 8. X-ray diffraction patterns of mixtures of YSZ and GDC electrolyte materials with cathode materials a) La_2NiO_4, b) $La_2Ni_{0.7}Co_{0.3}O_4$ and c) Pr_2NiO_4 subjected to heat treatment at 900 °C for 5 hours.

T a b l e 3

Interaction of materials based on La_2NiO_4 and Pr_2NiO_4 with electrolytes

Designation	Cathode material	Electrolyte	$T_{sintering}$, °C	Interaction
LN: YSZ	La_2NiO_4	YSZ	900	41 % secondary phase
LN: GDC	La_2NiO_4	GDC	900	No
LNC-30: YSZ	$La_2Ni_{0.7}Co_{0.3}O_4$	YSZ	900	12 % secondary phase
LNC-30: GDC	$La_2Ni_{0.7}Co_{0.3}O_4$	GDC	900	8 % secondary phase
PN: YSZ	Pr_2NiO_4	YSZ	900	38 % secondary phase
PN: GDC	Pr_2NiO_4	GDC	900	37 % secondary phase

Thermal expansion

On Figure 9 shows the results of measuring the linear expansion of the studied cathode materials in the temperature range of 20-1200 °C.

In the literature, the values of the coefficient of thermal expansion (CTE) averaged over the entire temperature range are usually given. For example, the CTE of $La_2NiO_{4+\delta}$ is 13.0×10^{-6} K^{-1} (20-1000 °C) [3]. However, on the curves of linear expansion obtained by us, a not very obvious inflection is observed in the region of 850 °C. Therefore, the CTE of the studied samples was calculated both for the entire temperature range (20–1200 °C) and separately for the low temperature (200–850 °C) and high temperature (850–1200 °C) regions. The calculation results, together with the coefficients of determination R^2, are summarized in Table 4. It can be seen that the approximation consisting of two linear regions describes the experimental data better.
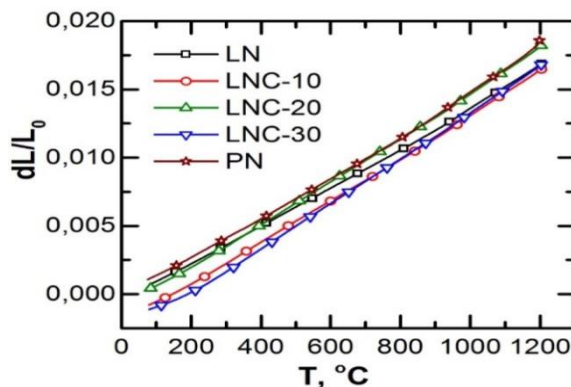
Figure 9. Temperature dependence of the change in the dimensions of samples of cathode materials.

T a b l e 4

Calculation of CTE for various temperature ranges

Compound	200-850 °C		850-1200 °C		20-1200 °C	
	TEC ($\times 10^{-6}$), K^{-1}	R^2	TEC ($\times 10^{-6}$), K^{-1}	R^2	TEC ($\times 10^{-6}$), K^{-1}	R^2
LN	13.89	0.99999	16.29	0.99822	14.39	0.99863
LNC-10	15.19	0.99992	16.81	0.99953	15.45	0.99932
LNC-20	15.72	0.99997	17.45	0.99901	15.93	0.99927
LNC-30	16.49	0.99993	17.51	0.99941	16.35	0.99978
PN	13.82	0.99991	16.50	0.99956	14.48	0.99788

Figure 10 shows the dependence of the change in CTE $La_2Ni_{1-x}Co_xO_{4+\delta}$ (x=0, 0.1, 0.2, 0.3) on the cobalt content for low- and high-temperature sections. It can be seen that with an increase in the content of cobalt in the composition of lanthanum nickelate, the CTE increases both in the low-temperature (20–800 °C) and high-temperature (800–1200 °C) regions. At the same time, in the low-temperature region, the introduction of cobalt has a stronger effect on the CTE of lanthanum nickelate than in the high-temperature region. Thus, from the point of view of CTE, LN and PN are the most suitable cathode materials with the Ruddlesden-Popper structure for YSZ and GDC electrolytes.
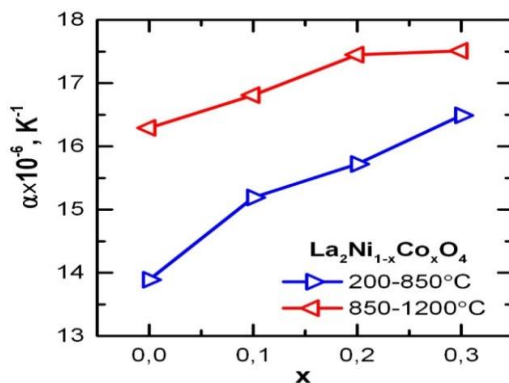
Figure 10. CTE of $La_2Ni_{1-x}Co_xO_{4+\delta}$ samples calculated for two temperature ranges 200-850 and 850-1200 °C

Conductivity

Figure 11 presents data on the total conductivity of the studied materials. It can be seen that a maximum is observed in the temperature dependences of the conductivity. According to [6], this behavior does not apply to the insulator-metal transition, but is due to the fact that at temperatures below 250 °C the chemical composition of $La_2NiO_{4+\delta}$ is stable and the change in conductivity reflects the behavior of the semiconductor type, that is, thermally activated Arrhenius-type conductivity. At higher temperatures, the materials lose some oxygen, which leads to a decrease in the M3+ content and, accordingly, a decrease in charge carrier densities and, consequently, a decrease in conductivity. Thus, competing phenomena (thermal activation and a decrease in the number of charge carriers) determine the presence of a maximum in the temperature dependence of the conductivity.
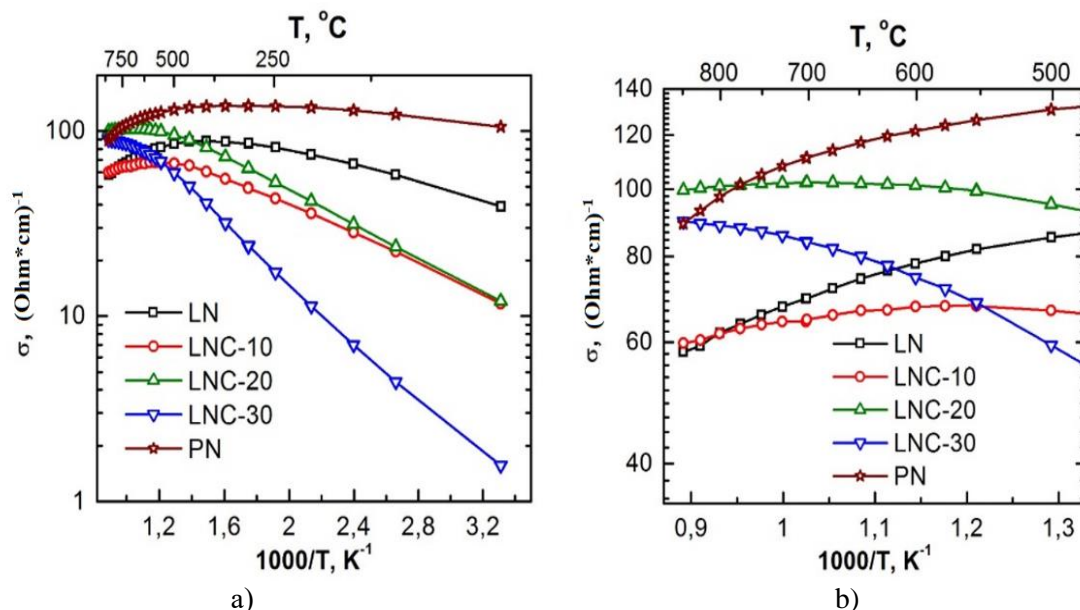
Figure 11. Temperature dependences of the conductivity of the studied materials:
a) — the entire temperature range, b) — high temperature range (500-850 °C).

If we compare the obtained data on the conductivity for the La_2NiO_4 material with the literature data [6, 9], it turns out that the value of the maximum conductivity is close — 80–90 S/cm. However, the temperature at which the maximum conductivity is reached differs significantly: in our study it is about 400 °C, while in [6, 9] it is about 650 °C.

It was shown in [9] that the conductivity of $La_2Ni_{1-x}Co_xO_{4+\delta}$, (x=0.1, 0.5, 1) decreases with increasing cobalt content. This was explained by the fact that in layered systems of the K_2NiF_4 type, the B-O-B bond is mainly responsible for the electrical properties [17]. Exchange interactions along the c axis are much weaker and occur through two oxygen ions. Consequently, with the introduction of cobalt, the Ni(Co)-O bond length increases, which leads to a weakening of the B-O covalent interaction and, consequently, to a decrease in electronic conductivity.

However, our study shows a different picture. If at x=0.1 the conductivity of $La_2Ni_{1-x}Co_xO_{4+\delta}$ decreases compared to $La_2NiO_{4+\delta}$, its value is 65 S/cm at 700 °C, which is close to the data of [9] — about 45 S/cm at 700 °C. Then at x=0.2 and 0.3, although there is a decrease in conductivity in the low-temperature region (which can be explained by the reason described above), in the high-temperature region, the conductivity increases. Most likely, this phenomenon is associated with the presence of a secondary phase observed in the LNC-20 and LNC-30 samples (section 2.1).

Figure 11 shows that PN has a higher conductivity compared to materials based on lanthanum nickelate in the temperature range of 20-800 °C. The obtained values of the conductivity PN and its temperature dependence correlate with the literature data [3, 18-19].

Thus, from the point of view of conductivity, the most suitable materials for a non-porous cathode are PN and LNC-20.

Polarization resistance.

On Figure 12 shows the impedance spectrum of a sample with LNC-10 electrodes. The shape of the spectrum is typical for all studied compositions and measurement temperatures, except for the sample with LNC-30 electrodes sintered to YSZ at 900 °C. For this sample, it was impossible to distinguish the components Rel-ta and Rη in the spectrum, so its polarization resistance is not discussed further. The method for calculating the polarization resistance of cathodes is described in Section 1.6.
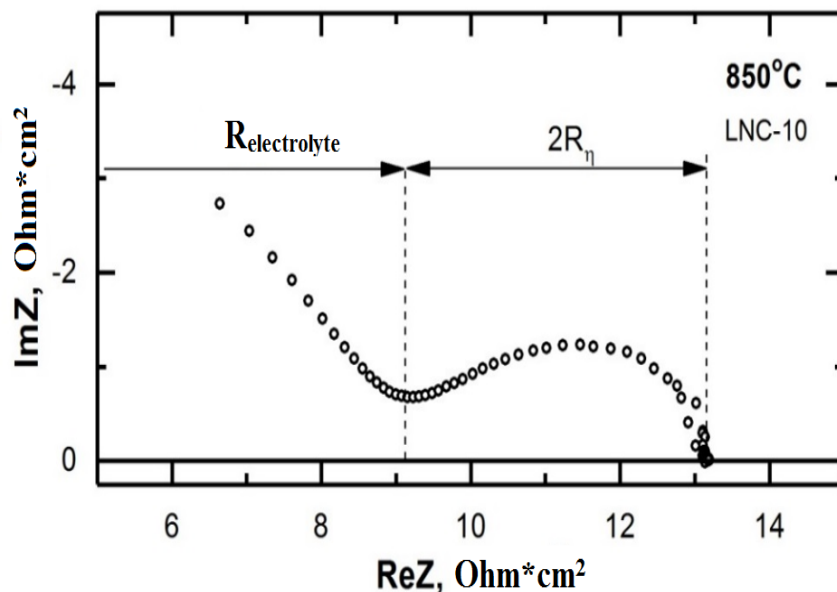
Figure 12. Impedance spectrum of a symmetrical sample with LNC-10 electrodes taken at 850 °C.
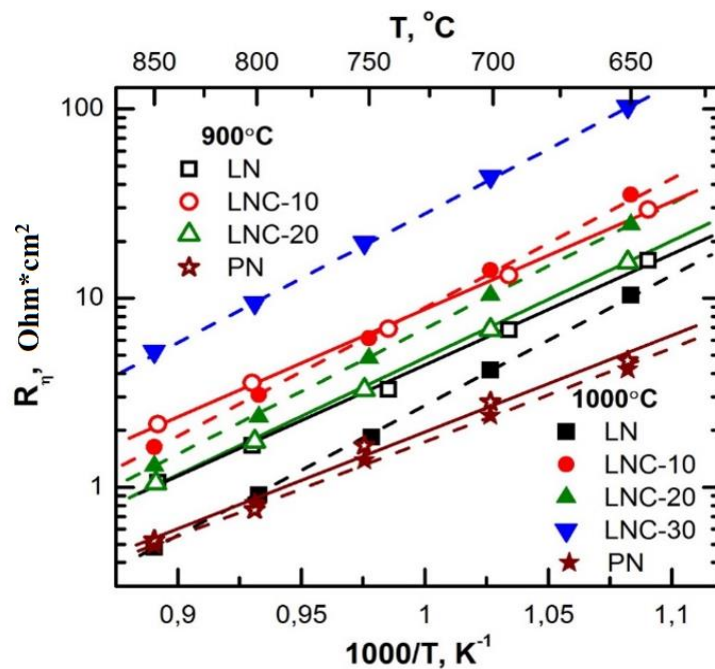
Figure 13. Temperature dependences of the polarization resistance of cathode materials sintered at 900 and 1000 °C.

Figure 13 shows the temperature dependences of the polarization resistance of the investigated cathodes. It can be seen that the electrodes sintered at 1000 °C are characterized by a lower polarization resistance than the electrodes sintered at 900 °C. Most likely, this is due to the formation of a better electrode-electrolyte contact. At the same time, LN and PN materials are characterized by the lowest polarization resistance. The introduction of Co into the composition of lanthanum nickelate leads to an increase in the polarization resistance of the cathode, however, this dependence is not linear.
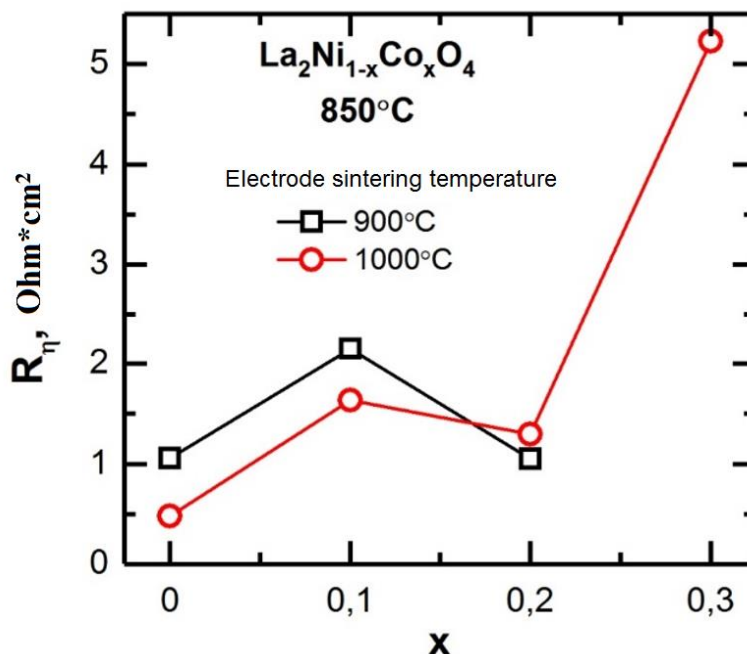
Figure 14. Dependence of polarization resistance of $La_2Ni_{1-x}Co_xO_{4+\delta}$ cathodes sintered to YSZ electrolyte at 900 and 1000 °C on cobalt content (x).

Figure 14 shows the dependence of the polarization resistance of $La_2Ni_{1-x}Co_xO_{4+\delta}$ cathodes on the cobalt content (x). It can be seen that the dependence is complex and non-linear. This is explained by the fact that the introduction of cobalt affects two characteristics of the material at once: conductivity and sintering kinetics. In the course of work on this project in 2018, it was shown that an increase in the content of Co in the composition of lanthanum nickelate leads to a shift in the shrinkage curve to a high-temperature region. Thus, the contact of the cathode material with the YSZ electrolyte formed at the same temperature should deteriorate with increasing Co in the LNC composition. On the other hand, according to the literature data [10, 20], the introduction of cobalt into the composition of La_2NiO_4 should lead to an increase in the oxygen diffusion coefficient and, thus, to a decrease in the polarization resistance. As shown above (see paragraph 2.4), the addition of 10 mol. % Co leads to a decrease in conductivity, which also affects the polarization resistance. While the conductivity of LNC-20 at high temperatures is higher than LN. However, the adhesion of the cathode to the YSZ electrolyte adversely affects the polarization resistance. Consequently, the "confrontation" of two factors (conductivity and sintering kinetics) causes a local minimum of polarization resistance at a content of 20 mol.% Co in the composition of $La_2NiO_{4+\delta}$.

Table 5 summarizes the data on the polarization resistance of the studied cathode materials with the Ruddlesden-Popper structure at 800 °C, and also presents the literature data. The Table shows data on electrodes baked at 1000 °C. As mentioned earlier, solid electrolytes based on CeO2 are more chemically inert to interaction with cathode materials than YSZ. Therefore, in the literature, the polarization resistance of cathodes with the K_2NiF_4 structure is studied mainly in contact with electrolytes based on CeO_2. As can be seen from Table 5, the polarization resistances of our cathodes in contact with the YSZ electrolyte are comparable with the literature data, in which the polarization of the cathodes was studied in contact with the CeO_2-based electrolyte.

Table 5

Polarization resistances of electrodes with the Ruddlesden-Popper structure at 800 °C.

Electrode	Electrolyte	R_η, Ohm*cm^2	Reference
$La_2NiO_{4+\delta}$	YSZ	0.9	this work
$La_2Ni_{0,9}Co_{0,1}O_{4+\delta}$	YSZ	3.0	this work
$La_2Ni_{0,8}Co_{0,2}O_{4+\delta}$	YSZ	2.4	this work
$La_2Ni_{0,7}Co_{0,3}O_{4+\delta}$	YSZ	5.2	this work
$Pr_2NiO_{4+\delta}$	YSZ	0.8	this work
$La_2NiO_{4+\delta}$	SmDC	0.2	[21]
$La_2Ni_{0,9}Co_{0,1}O_{4+\delta}$	GDC	3.0	[7]

Thus, the LN and PN materials have the highest catalytic activity among the studied ones.

Conclusions

As a result of the study, the following cathode materials were investigated: $La_2Ni_{1-x}Co_xO_4$ ($0 \leq x \leq 0.3$), Pr_2NiO_4. In this case, the influence of low concentrations of Co on the characteristics of lanthanum nickelate was studied for the first time. Materials based on lanthanum nickelate and praseodymium nickelate were characterized by a structure of the K_2NiF_4 type (Ruddlesden-Popper phases) with rhombic symmetry. Ruddlesden-Popper materials have been shown to be chemically compatible with $Zr_{0.84}Y_{0.16}O_{2-\delta}$ (YSZ) and $Ce_{0.73}Gd_{0.27}O_{2-\delta}$ (GDC) (GDC) electrolyte materials.

A study of the thermal expansion of cathode materials showed that all the studied materials are characterized by higher CTEs than YSZ and GDC electrolytes. Based on the studies performed, cathode materials were chosen for the formation of composites with GDC electrolyte: La_2NiO_4, $La_2Ni_{0.8}Co_{0.2}O_4$, Pr_2NiO_4. A study of the sintering kinetics and CTE of composites showed that their thermal characteristics are much closer to those of electrolytes than those of pure cathode materials.

Financing

References

1 Ivanov M. Laser synthesis of oxide nanopowders / M. Ivanov, V. Osipov, Yu. Kotov et al. // Advances in Science and Technology. — 2006. — No. 45. — P. 291–296.

2 Чупахина Т.И. Синтез, структурные и морфологические характеристики ультрадисперсных порошков и керамики на основе твердых растворов La2-xSr0.125PrxNiO4 (0 ≤ x ≤ 1.775). / Т.И. Чупахина, О.И. Гырдасова, Г.В. Базуев // Известия РАН. Серия Физическая. — 2013. — Т. 77. № 9. — С. 1276–1280.

3 Boehm E. Oxygen diffusion and transport properties in non-stoichiometric $Ln_{2-x}NiO_{4+\delta}$ oxides. Solid State Ionics / E. Boehm, J.-M. Bassat, P. Dordor et al. — 2005. — No. 176. — P. 2717–2725.

4 Mohan Ram R.A. Preparation and characterization of $La_2CoO_{4+\delta}$. / R.A. Mohan Ram, P. Ganguly, C.N.R. Rao // Materials Research Bulletin. — 1988. — No. 23. — P. 501-505.

5 Hayashi A. Successive structural phase transitions in stoichiometric La_2NiO_4 observed by X-ray diffraction / A. Hayashi, H. Tamura, Y. Ueda. — Physica C. — 1993. — No. 216. — P. 77-82.

6 Boehm E. Oxygen transport properties of $La_2Ni_{1-x}Cu_xO_{4+\delta}$ mixed conducting oxides / E. Boehm, J.-M. Bassat, M.C. Steil, et al. // Solid State Sciences. — 2003. — No. 5. — P. 973–981.

7 Amow G. Structural and sintering characteristics of the $La_2Ni_{1-x}Co_xO_{4+\delta}$ series / G. Amow, P.S. Whitfield, I.J. Davidson, R.P. Hammond // Ceramics International. — 2004. — No. 30. — P. 1635–1639.

8 Kilner J.A. Mass transport in $La_2Ni_{1-x}Co_xO_{4+\delta}$ oxides with the K_2NiF_4 structure / J.A. Kilner, C.K.M. Shaw // Solid State Ionics. — 2002. — P. 154–155, 523–527.

9 Amow, G. Structural and physical property trends of the hyperstoichiometric series $La_2Ni_{(1-x)}Co_xO_{4+\delta}$. / G. Amow, P.S. Whitfield, I.J. Davidson, et al. // Materials Research Society Symposia Proceedings. Solid State Inorganic Materials IV. — 2002. — P. 755, DD8.10.1-6.

10 Munnings C.N. Oxygen transport in the $La_2Ni_{1-x}Co_xO_{4+d}$ system / C.N. Munnings, S.J. Skinner, G. Amow, et al. // Solid State Ionics. — 2005. — No. 176. — P. 1895 — 1901.

11 Tsipis E.V. Electrode materials and reaction mechanisms in solid oxide fuel cells: a brief review. II. Electrochemical behavior vs. materials science aspects / E.V. Tsipis, V.V. Kharton // Journal of Solid State Electrochemistry. — 2008. — No. 12. — P. 1367–1391.

12 Mahato N. Progress in material selection for solid oxide fuel cell technology: A review / N. Mahato, A. Banerjee, A. Gupta, et al. // Progress in Materials Science. — 2015. — No. 72. — P. 141–337.

13 Zhao H. New cathode materials for ITSOFC: Phase stability, oxygen exchange and cathode properties of $La_{2-x}NiO_{4+\delta}$. / H. Zhao, F. Mauvy, et al. // Solid State Ionics. — 2008. — No. 179. — P. 2000–2005.

14 Hernandez A.M. $La_2NiO_{4+\delta}$ as cathode for SOFC: Reactivity study with YSZ and CGO electrolytes / A.M. Hernandez, L. Mogni, et al. // International Journal of Hydrogen Energy. — 2010. — No. 35. — P. 6031–6036.

15 Montenegro-Hernandez A. Thermal stability of $Ln_2NiO_{4+\delta}$ (Ln=La, Pr, Nd) and their chemical compatibility with YSZ and CGO solid electrolytes / A. Montenegro-Hernandez, J. Vega-Castillo, et al. // International Journal of Hydrogen Energy. — 2011. — No. 36. — P. 15704–15714.

16 Nikonov A.V. A brief review of conductivity and thermal expansion of perovskite-related oxides for SOFC cathode / A.V. Nikonov, K.A. Kuterbekov, Bekmyrza et al. // Eurasian Journal of Physics and Functional Materials. — 2018. — No. 2. — P. 274-292.

17 Richter J. Materials design for perovskite SOFC cathodes. / J. Richter, P. Holtappels et al. // Monatshefte für Chemie. — 2009. — No. 140. — P. 985–999.

18 Sadykov V.A. Tailoring the structural, thermal and transport properties of $Pr_2NiO_{4+\delta}$ through Ca-doping strategy / V.A. Sadykov, E.Yu. Pikalova, Z.S. Vinokurov et al. // Solid State Ionics. — 2019. — No. 333. — P. 30–37.

19 Rakhadilov B.K. Research of regimes of applying coats by the method of plasma electrolytic oxidation on Ti-6Al-4V / B.K. Rakhadilov, D.R. Baizhan, Zh.B. Sagdoldina, K. Torebek // Bulletin of the University of Karaganda-Physics. — 2022. — No. 1(105). — P. 99-106.

20 Zhao H. Ln_2MO_4 cathode materials for solid oxide fuel cells / H. Zhao, Q. Li, L. Sun // Science China Chemistry. — 2011. — No. 54. — P. 898–910.

21 Kolchugin A.A. Structural, electrical and electrochemical properties of calcium-doped lanthanum nickelate / A.A. Kolchugin, E.Yu. Pikalova, N.M. Bogdanovich et al. — Solid State Ionics. — 2016 — No. 288. — P. 48–53.

К.А. Кутербеков, К.Ж. Бекмырза, А.М. Кабышев,
М.М. Кубенова, Н.К. Айдарбеков, С.А. Нуркенов

Қатты оксидті отын элементтеріне арналған Радлесден-Поппер құрылымы бар материалдардың сипаттамаларын зерттеу

Мақалада $La_2Ni_{1-x}Co_xO_{4+\delta}$ (0≤x≤0.3) және $Pr_2NiO_{4+\delta}$ лантан никелаты негізіндегі материалдардың сипаттамаларын зерттеу нәтижелері келтірілген. Олардың кристалдық құрылымы және ysz және GDC электролиттік материалдарымен өзара әрекеттесуі 900 °C температурада талданды. Сондай-ақ, ysz электролиттік материалымен байланыста осы материалдардың поляризациялық кедергісі өлшенді. $La_2Ni_{1-x}Co_xO_4$ (0≤ x ≤0.3), Pr_2NiO_4 катод материалдары зерттелген. Бұл жағдайда Co-ның төмен концентрациясының лантан никелатының сипаттамаларына әсері алғаш рет қарастырылған. Лантан никелаты мен празеодим никелатына негізделген материалдар ромбтық симметриямен K_2NiF_4 типті (Радлсден-Поппер фазасы) құрылымымен сипатталды. Радлсден-Поппер құрылымы бар материалдар $Zr_{0.84}Y_{0.16}O_{2-\delta}$ (YSZ) және $Ce_{0.73}Gd_{0.27}O_{2-\delta}$ (GDC) электролиттік материалдармен химиялық үйлесімді екендігі көрсетілген. Катодты материалдардың термиялық кеңеюін зерттеу барлық зерттелетін материалдар YSZ және GDC электролиттеріне қарағанда жоғары ТКК-мен сипатталатыны дәлелденген. Жүргізілген зерттеулер негізінде GDC электролиті бар композиттерді қалыптастыру үшін келесі катодты материалдар таңдалды: La_2NiO_4, $La_2Ni_{0.8}Co_{0.2}O_4$, Pr_2NiO_4. Композиттердің агломерация кинетикасы мен ТКК зерттеуі — олардың термиялық сипаттамалары таза катодты материалдарға қарағанда электролиттердің сипаттамаларына едәуір жақын екенін көрсетті.

Кілт сөздер: ҚООЭ, катодты материалдар, өткізгіштік, температуралық кеңею коэффициенті, нано ұнтақтар.

К.А. Кутербеков, К.Ж. Бекмырза, А.М. Кабышев,
М.М. Кубенова, Н.К. Айдарбеков, С.А. Нуркенов

Исследование характеристик материалов со структурой Раддлсдена-Поппера для твердооксидных топливных элементов

В статье представлены результаты исследования характеристик материалов на основе никелата лантана La2Ni1-xCoxO4+δ (0≤x≤0,3) и Pr2NiO4+δ. Проанализированы их кристаллическая структура и взаимодействие с электролитными материалами YSZ и GDC при 900 °C. Определены коэффициенты термического расширения и исследованы температурные зависимости проводимостей. А также измерено поляризационное сопротивление данных материалов в контакте с электролитным материалом YSZ. Были исследованы следующие катодные материалы: La2Ni1-xCoxO4 (0≤ x ≤0,3), Pr2NiO4. При этом впервые было изучено влияние малых концентраций Co на характеристики никелата лантана. Материалы на основе никелата лантана и никелата празеодима характеризовались структурой типа K_2NiF_4 (фазы Раддлсдена-Поппера) с ромбической симметрией. Было показано, что материалы со структурой Раддлсдена-Поппера химически совместимы с электролитными материалами $Zr_{0.84}Y_{0.16}O_{2-δ}$ (YSZ) и $Ce_{0.73}Gd_{0.27}O_{2-δ}$ (GDC). Исследование термического расширения катодных материалов показало, что все исследуемые материалы характеризуются более высокими КТР, чем электролиты YSZ и GDC. На основании проведенных исследований были выбраны катодные материалы для формирования композитов с электролитом GDC: La_2NiO_4, $La_2Ni_{0.8}Co_{0.2}O_4$, Pr_2NiO_4. Исследование кинетики спекания и КТР композитов показало, что их термические характеристики значительно ближе к характеристикам электролитов, чем у чистых катодных материалов.

Ключевые слова: ТОТЭ, катодные материалы, проводимость, коэффициент температурного расширения, нанопорошки.

References

1 Ivanov, M., Osipov, V., Kotov, Yu. et al. (2006). Laser synthesis of oxide nanopowders. *Advances in Science and Technology, 45, 291–296.*

2 Chupahina, T.I., Gyrdasova, O.I., & Bazuev, G.V. (2013). Sintez, strukturnye i morfologicheskie kharakteristiki ultradispersnykh poroshkov i keramiki na osnove tverdykh rastvorov La2-xSr0.125PrxNiO4 (0 ≤ x ≤ 1.775) [Synthesis, structural and morphological characteristics of ultrafine powders and ceramics based on solid solutions La2-xSr0.125PrxNiO4 (0 ≤ x ≤ 1.775)]. *Izvestiia Rossiiskoi akademii nauk. Seriia Pizicheskaia — The journal Izvestia of the Russian Academy of Sciences. The series physical, 77, 9, 1276–1280* [in Russian].

3 Boehm, E., Bassat, J.-M., Dordor, P. et al. (2005). Oxygen diffusion and transport properties in non-stoichiometric Ln2-xNiO4+δ oxides. *Solid State Ionics, 176, 2717–2725.*

4 Mohan Ram, R.A., Ganguly, P., Rao, C.N.R. (1988). Preparation and characterization of La2CoO4+δ. *Materials Research Bulletin, 23, 501-505.*

5 Hayashi, A., Tamura, H., Ueda, Y. (1993). Successive structural phase transitions in stoichiometric La2NiO4 observed by X-ray diffraction. *Physica C, 216, 77-82.*

6 Boehm, E., Bassat, J.-M., Steil, M.C. et al. (2003). Oxygen transport properties of La2Ni1−xCuxO4+δ mixed conducting oxides. *Solid State Sciences, 5, 973–981.*

7 Amow, G., Whitfield, P.S., Davidson, I.J., Hammond, R.P. (2004). Structural and sintering characteristics of the La2Ni1−xCoxO4+δ series. *Ceramics International, 30, 1635–1639.*

8 Kilner, J.A., Shaw, C.K.M. (2002) Mass transport in La2Ni1-xCoxO4+δ oxides with the K2NiF4 structure. *Solid State Ionics, 154–155, 523– 527.*

9 Amow, G., Whitfield, P.S., Davidson, I.J., et al. (2002). Structural and physical property trends of the hyperstoichiometric series La2Ni(1−x)CoxO4+δ. Materials Research Society Symposia Proceedings. *Solid State Inorganic Materials IV, 755, DD8.10.1-6.*

10 Munnings, C.N., Skinner, S.J., Amow, G., et al. (2005). Oxygen transport in the La2Ni1−xCoxO4+d system. *Solid State Ionics, 176, 1895—1901.*

11 Tsipis, E.V., Kharton, V.V. (2008). Electrode materials and reaction mechanisms in solid oxide fuel cells: a brief review. II. Electrochemical behavior vs. materials science aspects. *Journal of Solid State Electrochemistry, 12, 1367–1391.*

12 Mahato, N., Banerjee, A., Gupta, A. et al. (2015). Progress in material selection for solid oxide fuel cell technology: A review. *Progress in Materials Science, 72, 141–337.*

13 Zhao, H., Mauvy, F. et al. (2008). New cathode materials for ITSOFC: Phase stability, oxygen exchange and cathode properties of La2-xNiO4+δ. *Solid State Ionics, 179, 2000–2005.*

14 Hernandez, A.M., Mogni, L. et al. (2010). La2NiO4+δ as cathode for SOFC: Reactivity study with YSZ and CGO electrolytes. *International Journal of Hydrogen Energy, 35, 6031–6036.*

15 Montenegro-Hernandez, A., Vega-Castillo, J. et al. (2011). Thermal stability of Ln2NiO4+δ (Ln=La, Pr, Nd) and their chemical compatibility with YSZ and CGO solid electrolytes. *International Journal of Hydrogen Energy, 36, 15704–15714.*

16 Nikonov, A.V., Kuterbekov, K.A., Bekmyrza, K.Zh., Pavzderin, N.B. (2018). A brief review of conductivity and thermal expansion of perovskite-related oxides for SOFC cathode. *Eurasian Journal of Physics and Functional Materials, 2, 274-292.*

17 Richter, J., Holtappels, P. et al. (2009). Materials design for perovskite SOFC cathodes. *Monatshefte für Chemie, 140, 985–999.*

18 Sadykov, V.A., Pikalova, E.Yu., Vinokurov, Z.S. et al. (2019). Tailoring the structural, thermal and transport properties of $Pr_2NiO_{4+\delta}$ through Ca-doping strategy. *Solid State Ionics, 333, 30–37.*

19 Rakhadilov, B.K., Baizhan, D.R., Sagdoldina, Zh.B., Torebek, K. (2022). Research of regimes of applying coats by the method of plasma electrolytic oxidation on Ti-6Al-4V. *Bulletin of the University of Karaganda-Physics, 1(105), 99-106.*

20 Zhao, H., Li, Q., Sun, L. (2011). Ln_2MO_4 cathode materials for solid oxide fuel cells. *Science China Chemistry, 54, 898–910.*

21 Kolchugin, A.A., Pikalova, E.Yu., Bogdanovich, N.M. et al. (2016). Structural, electrical and electrochemical properties of calcium-doped lanthanum nickelate. *Solid State Ionics, 288, 48–53.*